

Figure 1: (a) **Illustration of the multivariate, geo-tagged time series imputation task**: the input data has three dimensions (i.e. time, location, measurement) with some missing values (indicated by the orange dot); the output is of same shape as the input while the missing values have been imputed (indicated by the red dot). (b) **Self-attention mechanism**: the **Attention Map** is first computed using every pair of **Query** vector and **Key** vector and then guides the updating of **Value** vectors via weighted sum to take into account contextual information. (c) **Traditional Self-Attention** mechanism updates Value vector along the temporal dimension only vs. **Cross-Dimensional Self-Attention** mechanism updates Value vector according to data across all dimensions.

relationship based on RNN Cho et al. [2014b]; Hochreiter and Schmidhuber [1997]; Cho et al. [2014a]. However, due to the constraint of sequential computation over time, the training of RNN cannot be parallelized and thus is usually time-consuming. Moreover, the relationship between each two distant time stamps cannot be directly modeled. Recently, the self-attention mechanism as shown in Fig. 1(b) has been proposed by the seminal work of *Transformer* Vaswani et al. [2017] to get rid of the limitation of sequential processing, accelerating the training time substantially and improving the performance significantly on seq-to-seq tasks in Natural Language Processing (NLP) because the relevance between each two time stamps is captured explicitly.

In this paper, we are the first to adapt the self-attention mechanism to impute missing data in multivariate time series, which cover multiple geo-locations and contain multiple measurements as shown in Fig. 1(a). In order to impute a missing value in such unique multi-dimensional data, it is very useful to look into available data in different dimensions (i.e. **time**, **location** and **measurement**), as shown in Fig. 1(c). To this end, we investigate several choices of modeling self-attention across different dimensions. In particular, we propose a novel Cross-Dimensional Self-Attention (CDSA) mechanism to capture the attention crossing all dimensions jointly yet in a decomposed, computationally inexpensive manner. In summary, we make the following contributions:

- (i) We are the first to apply the self-attention mechanism to the multivariate, geo-tagged time series data imputation task, replacing the conventional RNN-based models to speed up training and directly model the relationship between each two data values in the input data.
- (ii) For the unique time series data of multiple dimensions (i.e. **time**, **location**, **measurement**), we comprehensively study several choices of modeling self-attention crossing different dimensions. Our CDSA mechanism models self-attention crossing all dimensions jointly yet in a dimension-wise decomposed way. We show that CDSA is computationally efficient and independent with the order of processing each dimension.
- (iii) We extensively evaluate on three standard benchmarks and our newly collected traffic dataset. Experimental results show that our model outperforms the state-of-the-art models for both data imputation and forecasting tasks.

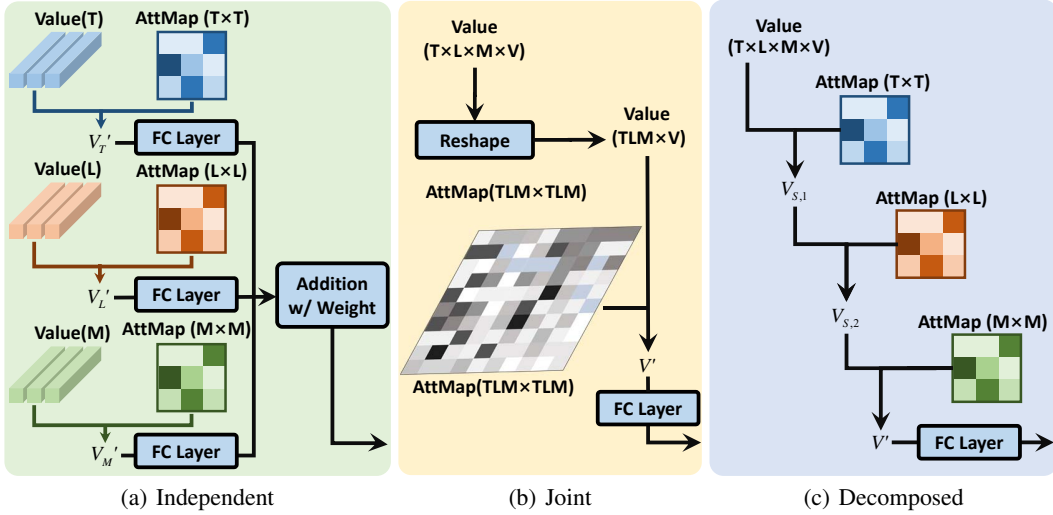


Figure 2: Three choices of implementing our Cross-Dimensional Self-Attention mechanism

## 2 Related Work

**Statistical data imputation methods.** Statistical methods Ansley and Kohn [1984]; Zhang [2003]; Shumway and Stoffer [1982]; Nelwamondo et al. [2007]; Buuren and Groothuis-Oudshoorn [2010] often impose assumptions over data and reconstruct the missed value by fitting a *smooth curve* to the available values. For instance, Kriging variogram model Stein [2012] was proposed to capture the variance in data w.r.t. the geodesic distance. Matrix completion methods Acuna and Rodriguez [2004]; Yu et al. [2016]; Friedman et al. [2001]; Cai et al. [2010]; Ji and Ye [2009]; Ma et al. [2011] usually enforce low-rank constraint.

**RNN-based data imputation methods.** Li et al. [2018] proposed DCGRU for seq-to-seq by adopting graph convolution Chung and Graham [1997]; Shi [2009]; Shuman et al. [2012] to model spatio-temporal relationship. Luo et al. [2018] built GRUI by incorporating RNN into a Generative Adversarial Network (GAN). Cao et al. [2018] utilized bi-directional RNN and treated the missing values as trainable variables. Nevertheless, these RNN-based models fundamentally suffer from the constraint of sequential processing, which leads to long training time and prohibits the direct modeling of the relationship between two distant data values.

**Self-attention.** Recently, Vaswani et al. [2017] introduced the *Transformer* framework which entirely rely on self-attention, learning the association between each two words in a sentence. Then self-attention has been widely applied in seq-to-seq tasks such as machine translation, image generation Yang et al. [2016]; Zhang et al. [2018a] and graph-structured data Veličković et al. [2017]. In this paper, we are the first to apply self-attention for multi-dimensional data imputation and specifically we investigate several choices of modeling self-attention crossing different data dimensions.

## 3 Approach

In Sec. 3.1, we first review the conventional self-attention mechanism in NLP. In Sec. 3.2, we propose three methods for computing attention map cross different dimensions. In Sec. 3.3 and 3.4, we present details of using CDSA for missing data imputation.

### 3.1 Conventional Self-Attention

As shown in Fig. 1(b), for language translation task in NLP, given an input sentence, each word  $x_i$  is mapped into a *Query* vector  $q_i$  of  $d$ -dim, a *Key* vector  $k_i$  of  $d$ -dim, and a *Value* vector  $v_i$  of  $v$ -dim. The attention from word  $x_j$  to word  $x_i$  is effectively the scaled dot-product of  $q_i$  and  $k_j$  after Softmax,

which is defined as  $\mathbf{A}(i, j) = \exp(\mathbf{S}(i, j)) \left( \sum_{j=1}^T \exp(\mathbf{S}(q, j)) \right)^{-1}$  where  $\mathbf{S}(i, j) = \mathbf{q}_i \mathbf{k}_j^\top / \sqrt{d}$ . Then,  $\mathbf{v}_i$  is updated to  $\mathbf{v}'_i$  as a weighted sum of all the *Value* vectors, defined as  $\mathbf{v}'_i = \sum_{j=1}^T \mathbf{A}(i, j) \mathbf{v}_j$ , after which each  $\mathbf{v}'_i$  is mapped to the layer output  $\mathbf{x}'_i$  of the same size as  $\mathbf{x}_i$ . In order to adapt the self-attention from NLP to our multivariate, geo-tagged time series data, a straightforward way is to view all data in a time stamp as one word embedding and model the self-attention over time.

### 3.2 Cross-Dimensional Self-Attention

In order to model Cross-Dimensional Self-Attention (CDSA), in this section we propose three solutions: (1) model attention within each dimension **independently** and perform late fusion; (2) model attention crossing all dimensions **jointly**; (3) model attention crossing all dimensions in a joint yet **decomposed** manner. We assume the input data  $\mathcal{X} \in \mathbb{R}^{T \times L \times M}$  has three dimensions corresponding time, location, measurement.  $\mathcal{X}$  can be reshaped into two-dimensional matrices (i.e.  $\mathbf{X}_T \in \mathbb{R}^{T \times LM}$ ,  $\mathbf{X}_L \in \mathbb{R}^{L \times MT}$ ,  $\mathbf{X}_M \in \mathbb{R}^{M \times TL}$ ) or an one-dimensional vector (i.e.  $\mathbf{X} \in \mathbb{R}^{TLM \times 1}$ ). Similarly, this superscript may be applied on the *Query*, *Key* and *Value*, e.g.,  $\mathbf{Q} \in \mathbb{R}^{T \times L \times M \times d}$ ,  $\mathbf{Q}_L \in \mathbb{R}^{L \times MT \times d}$  and  $\mathbf{Q} \in \mathbb{R}^{TLM \times d}$ .

#### 3.2.1 Independent

As shown in Fig. 2(a), the input  $\mathcal{X}$  is reshaped into three input matrices  $\mathbf{X}_T$ ,  $\mathbf{X}_L$  and  $\mathbf{X}_M$ . Three streams of self-attention layers are built to process each input matrix in parallel. Such as the first layer in stream on  $\mathbf{X}_L$ , each vector  $\mathbf{X}_L(l, :)$  of  $MT$ -dim is viewed as a word vector in NLP. Following the steps in Sec. 3.1,  $\mathbf{X}_L(l, :)$  is mapped to  $\mathbf{Q}_L(l, :)$  and  $\mathbf{K}_L(l, :)$  of  $d_L$ -dim, as well as  $\mathbf{V}_L(l, :)$  of  $v_L$ -dim. The output of every stream's last layer are fused through element-wise addition,  $\mathcal{X}' = \alpha_T \mathcal{X}'_T + \alpha_L \mathcal{X}'_L + \alpha_M \mathcal{X}'_M$ , where the weights  $\alpha_T$ ,  $\alpha_L$  and  $\alpha_M$  are trainable parameters. Besides, the hyper-parameters for each stream such as the number of layers, are set separately.

#### 3.2.2 Joint

As shown in Fig. 2(b), the three-dimensional input  $\mathcal{X}$  is reshaped as to  $\mathbf{X}$ . Each unit  $\mathbf{X}(p)$  is mapped to  $\mathbf{Q}(p, :)$  and  $\mathbf{K}(p, :)$  of  $d$ -dim as well as  $\mathbf{V}(p, :)$  of  $v$ -dim, where  $p = p(t, l, m)$  denotes the index mapping from the 3-D cube to the vector form. In this way, an attention map of dimension  $TLM \times TLM$  is built to directly model the cross-dimensional interconnection.

#### 3.2.3 Decomposed

The *Independent* manner sets multiple attention sub-layers in each stream to model the dimension-specific attention but fail in modeling cross-dimensional dependency. In contrast, the *Joint* manner learns the cross-dimensional relationship between units directly but results in huge computation workload. To capture both the dimension-specific attention and cross-dimensional attention in a distinguishable way, we propose a novel *Decomposed* manner.

As shown in Fig. 2(c), the input  $\mathcal{X}$  is reshaped as input matrices  $\mathbf{X}_T$ ,  $\mathbf{X}_L$ ,  $\mathbf{X}_M$  and  $\mathbf{X}$ . Each unit  $\mathbf{X}(p)$  is mapped to vector  $\mathbf{V}(p, :)$  of  $v$ -dim as in the *Joint* while  $\mathbf{X}_T$ ,  $\mathbf{X}_L$  and  $\mathbf{X}_M$  are used for building attention map  $\mathbf{A}_T$ ,  $\mathbf{A}_L$ ,  $\mathbf{A}_M$  individually as in the *Independent*. The attention maps are applied on *Value* vector in order as,

$$\mathbf{V}' = \mathbf{A}\mathbf{V} = \tilde{\mathbf{A}}_M \mathbf{V}_{S,2} = \tilde{\mathbf{A}}_M \tilde{\mathbf{A}}_L \mathbf{V}_{S,1} = \tilde{\mathbf{A}}_M \tilde{\mathbf{A}}_L \tilde{\mathbf{A}}_T \mathbf{V}. \quad (1)$$

The attention map with  $\tilde{\phantom{A}}$  is reshaped from the original attention map and consistent with the calculation in (1), e.g.,  $\tilde{\mathbf{A}}_T \in \mathbb{R}^{TLM \times TLM}$  is reshaped from  $\mathbf{A}_T \in \mathbb{R}^{T \times T}$ . More specifically,

$$\begin{aligned} \tilde{\mathbf{A}}_T &= \mathbf{A}_T \otimes \mathbf{I}_L \otimes \mathbf{I}_M, \\ \tilde{\mathbf{A}}_L &= \mathbf{I}_T \otimes \mathbf{A}_L \otimes \mathbf{I}_M, \\ \tilde{\mathbf{A}}_M &= \mathbf{I}_T \otimes \mathbf{I}_L \otimes \mathbf{A}_M, \end{aligned} \quad (2)$$

where  $\otimes$  denotes *tensor product* and  $\mathbf{I}$  is the *Identity* matrix where the subscript indicates the size, e.g.,  $\mathbf{I}_T \in \mathbb{R}^{T \times T}$ . Although the three reshaped attention maps are applied with a certain order, according to (2), we show that each unit in  $\mathbf{A}$  is effectively calculated as

$$\mathbf{A}(p_0, p_1) = \mathbf{A}_T(t_0, t_1) \mathbf{A}_L(l_0, l_1) \mathbf{A}_M(m_0, m_1), \quad (3)$$

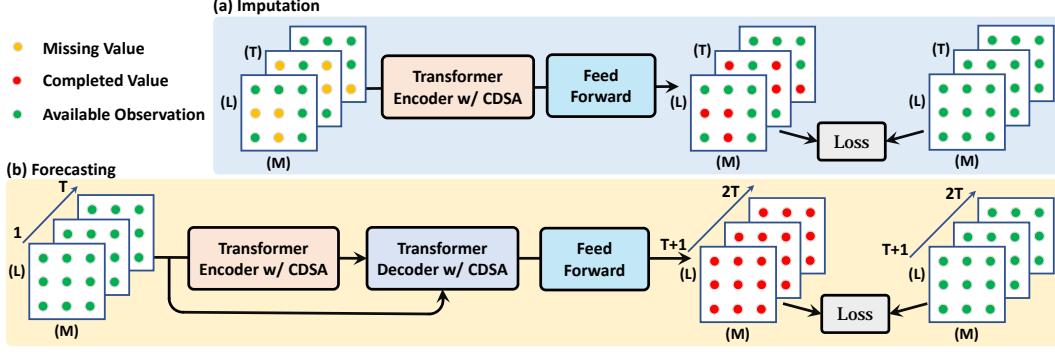


Figure 3: The framework employing CDSA for data imputation and forecasting.

where  $p_0 = p(t_0, l_0, m_0), p_1 = p(t_1, l_1, m_1)$ . Following the associativity of tensor product, we demonstrate

$$\tilde{\mathbf{A}}_{\sigma(L)} \tilde{\mathbf{A}}_{\sigma(M)} \tilde{\mathbf{A}}_{\sigma(T)} = \mathbf{A}_T \otimes \mathbf{A}_L \otimes \mathbf{A}_M, \quad (4)$$

where  $\sigma = \sigma(T, L, M)$  denotes the arbitrary arrangement of sequence (T, L, M), e.g., (T, M, L). Effectively, the arrangement  $\sigma$  is the order of attention maps to update  $\mathbf{V}$ . As (3)-(4) shows that the weight in  $\mathbf{A}$  is decomposed as the product of weights in three dimension-specific attention maps, the output and gradient back propagation are order-independent. Furthermore, we show in Supp that the cross-dimensional attention map has the following property:

$$\sum_{p_1=1}^{TLM} \mathbf{A}(p_0, p_1) = \sum_{t_1=1}^T \sum_{l_1=1}^L \sum_{m_1=1}^M \mathbf{A}_T(t_0, t_1) \mathbf{A}_L(l_0, l_1) \mathbf{A}_M(m_0, m_1) = 1. \quad (5)$$

In summary, the *Independent* builds attention stream for each dimension while the *Joint* directly model the attention map among all the units. Our proposed CDSA is based on the *Decomposed*, which forms a cross-dimensional attention map, out of three dimension-specific maps. As an alternative of the *Decomposed*, the *Shared* maps unit  $\mathbf{X}(p)$  to  $\mathbf{Q}(p, :)$  and  $\mathbf{K}(p, :)$  of  $d$ -dim and calculates all three dimension-specific attention map, e.g.,  $\mathbf{A}_L = \text{Softmax}(\mathbf{Q}_{(L)} \mathbf{K}_{(L)}^\top / \sqrt{MTd})$ . As shown in Table 1, by using Tensorflow *profile* and fixing the hyper-parameters with detailed explanations in Supp., the *Decomposed* significantly decreases the FLoating point OPERations (FLOPs) compared to the *Joint* and requires less variables than the *Independent*. Detailed comparisons are reported in Sec. 4.3.

Table 1: Computational complexity of several methods to implement CDSA

Methods	<i>Independent</i>	<i>Joint</i>	<i>Shared</i>	<i>Decomposed</i>
FLOPs ( $\times 10^9$ )	0.39	3.22	0.21	0.24
Number of Variables ( $\times 10^5$ )	18.15	0.44	0.44	16.09

### 3.3 Framework

**Imputation:** As shown in Fig. 3(a), we apply our CDSA mechanism in a *Transformer Encoder*, a stack of  $N = 8$  identical layers with residual connection He et al. [2016] and normalization Lei Ba et al. [2016] as employed by Vaswani et al. [2017]. To reconstruct the missing (along with other) values of the input, we apply a fully connected *Feed Forward* network on the final Value tensor, which is trained jointly with the rest of the model.

**Forecasting:** As shown in Fig. 3(b), we apply our CDSA mechanism in *Transformer* framework where we set  $N = 9$  for both encoder and decoder. Similar to imputation, we use a fully connected feed forward network to generate the predicted values.

### 3.4 Implementation Details

We normalize each measurement of the input by subtracting the mean and dividing by standard deviation across training data. Then the entries with missed value are set 0. We use the Adam

optimizer Kingma and Ba [2014] to minimize the Root Mean Square Error (RMSE) between the prediction and ground truth. The model is trained on a single NVIDIA GTX 1080 Ti GPU. More details (e.g., network hyper-parameters, learning rate and batch size) can be found in Supp.

## 4 Experiments

### 4.1 Datasets, Tasks, Evaluation Metrics

**NYC-Traffic.** New York City Department of Transportation has set up various street cameras<sup>2</sup>. Each camera keeps taking a snapshot every a few seconds. The is collected around 1-month data from 12/03/2015 to 12/26/2015 for 186 cameras on Manhattan. For each snapshot, we apply our trained faster-RCNN Ren et al. [2015] vehicle detection model to detect the number of vehicles (#vehicle) contained in each snapshot. To aggregate such raw data into time series, for every non-overlapping 5-minute window, we averaged #vehicle from each snapshot to obtain the average #vehicle as the only measurement. Finally, we obtained 186 time series where each value represents the average #vehicle and the gap between two consecutive time stamps is 5 minutes.

The natural missing rate of the whole dataset is 8.43%. In order to simulate experiments for imputation, we further remove some entries and hold them as ground truth for evaluation. The imputation task is to estimate values of these removed entries. To mimic the natural data missing pattern, we model our manual removal as a *Burst Loss*, which means at certain location the data is continuously missed for a certain period. More details about vehicle detection and burst loss are be found in Supp. To simulate various data missing extents, we vary the final missing rate after removal from 20% to 90%. For each missing rate, we randomly select 432 consecutive time slots to train our model and evaluate the average RMSE of 5 trials. The dataset will be released publicly.

**KDD-2015** Zheng et al. [2015]. This dataset focuses on air quality and meteorology. It contains data recorded hourly, ending up with totally 8,759 time stamps. PM2.5 measurement is recorded at 36 locations and Temperature and Humidity are recorded at 16 locations in Beijing from 05/01/2014 to 04/30/2015, with natural missing rate 13.3%, 21.1% and 28.9% respectively. We treat those two subsets as two separate tasks and evaluate our method on each task separately. Following Yi et al. [2016], data in 3<sup>rd</sup>, 6<sup>th</sup>, 9<sup>th</sup> and 12<sup>th</sup> months are for testing and the remaining months are for training. We randomly select 36 consecutive time slots to train our model and evaluate Mean Absolute Error (MAE) as well as Mean Relative Error (MRE).

In order to simulate experiments for imputation, besides the natural missing data, for PM2.5 we follow the strategy used in Yi et al. [2016]; Cao et al. [2018]; Zhou and Huang [2018] to further manually remove entries and hold their values as ground truth. The imputation task is to predict values of these manually removed entries. For Temperature and Humidity, we follow Zhou and Huang [2018] to randomly hold 20% of available data.

**KDD-2018** Cup [2018]. Like **KDD-2015**, **KDD-2018** is an Air Quality and Meteorology dataset recorded hourly from 01/01/2017 to 04/30/2017. As indicated in Luo et al. [2018], 11 locations and 12 measurements are selected. The natural missing rate is 6.83%. In order to simulate experiments for imputation, we follow Luo et al. [2018] to split the data to every 48 hours, randomly hold values of some available entries and vary the missing rate from 20% to 90%. Mean Squared Error (MSE) is used for evaluation.

**METR-LA** Jagadish et al. [2014]. We follow Li et al. [2018] to use this dataset for traffic speed forecasting. This dataset contains traffic speed at 207 locations recorded every 5 minutes for 4 months ranging from 03/01/2012 to 06/30/2012. Following Li et al. [2018], 80% of data at the beginning of these 4 months is used for training and the remaining 20% is for testing. In order to simulate the forecasting scenario, within either training or testing set, every time series of consecutive 2 hours are enumerated. For each time series, data in the first hour is treated as input and data in the second hour is to be predicted. We respectively evaluate the forecasting results at 15-th, 30-th, 60-th minutes in the second 1 hour and also evaluate the average evaluation results within the total 1 hour. We use RMSE, MAE and Mean Absolute Percentage Error (MAPE) as evaluation metrics.

---

<sup>2</sup><https://nycctmc.org/>

## 4.2 Comparisons with State-of-the-art

**NYC-Traffic.** In Table 2, our CDSA consistently outperforms traditional methods including Auto Regressive, Kriging expo, Kriging linear and a recent RNN-based method (i.e. MTSI, BRITS, DCRNN) over a wide range of missing rate. Because CDSA leverages the self-attention mechanism to avoid sequential processing of RNN and directly model the relationship between distant data. Detailed overview of baselines can be found in Supp.

**KDD-2015.** Table 3 shows that for PM2.5, our method outperforms the traditional methods significantly and achieves comparable MAE as IIN Zhou and Huang [2018] while better MRE than IIN Zhou and Huang [2018]. For Temperature and Humidity, our method consistently outperforms state-of-the-art methods.

Table 2: RMSE on dataset **NYC-Traffic** for comparisons with SOTA

Model \ Missing Rate	20%	30%	40%	50%	60%	70%	80%	90%
Auto Regressive	2.354	2.357	2.359	2.362	2.364	2.652	2.796	3.272
Kriging expo	2.142	2.145	2.157	2.152	2.155	2.165	2.182	2.231
Kriging linear	2.036	2.008	2.031	2.038	2.056	2.074	2.111	2.194
MTSI Luo et al. [2018]	1.595	1.597	1.603	1.605	1.608	1.641	1.672	1.834
BRITS Cao et al. [2018]	1.337	1.339	1.341	1.355	1.376	1.395	1.408	1.477
DCRNN Li et al. [2018]	1.397	1.399	1.401	1.419	1.432	1.443	1.459	1.601
<b>CDSA (ours)</b>	<b>1.203</b>	<b>1.208</b>	<b>1.211</b>	<b>1.214</b>	<b>1.215</b>	<b>1.217</b>	<b>1.234</b>	<b>1.377</b>

Table 3: MAE/MRE on dataset **KDD-2015** for comparisons with SOTA

Model \ Dataset	PM2.5		TEMP		HUM	
	MAE	MRE	MAE	MRE	MAE	MRE
Mean	55.51	77.97%	9.21	97.56%	20.34	57.85%
KNN	29.79	41.85%	1.26	19.83%	7.28	16.22%
MICE	27.42	38.52%	1.23	18.29%	6.97	15.87%
ST-MVL Yi et al. [2016]	12.12	17.40%	0.68	4.59%	3.37	5.91%
MTSI Luo et al. [2018]	13.34	18.01%	0.71	4.67%	3.51	6.21%
BRITS Cao et al. [2018]	11.56	16.65%	0.63	4.16%	3.31	5.68%
DCRNN Li et al. [2018]	12.33	17.82%	0.69	4.59%	2.95	5.12%
IIN Zhou and Huang [2018]	<b>10.63</b>	15.31%	0.63	4.22%	2.90	5.09%
<b>CDSA (ours)</b>	10.67	<b>14.89%</b>	<b>0.61</b>	<b>4.15%</b>	<b>2.81</b>	<b>4.92%</b>

Table 4: MSE on dataset **KDD-2018** for comparisons with SOTA

Model \ Missing Rate	20%	30%	40%	50%	60%	70%	80%	90%
Mean Filling	0.916	0.907	0.914	0.923	0.973	0.935	0.937	1.002
KNN Filling	0.892	0.803	0.776	0.798	0.856	0.852	0.873	1.243
MF Filling	0.850	0.785	0.787	0.772	0.834	0.805	0.860	1.196
MTSI Luo et al. [2018]	0.844	0.780	0.753	0.743	0.803	0.780	0.837	1.018
BRITS Cao et al. [2018]	0.455	0.421	0.372	0.409	0.440	0.482	0.648	0.725
DCRNN Li et al. [2018]	0.579	0.565	0.449	0.506	0.589	0.622	0.720	0.861
<b>CDSA (ours)</b>	<b>0.373</b>	<b>0.393</b>	<b>0.287</b>	<b>0.291</b>	<b>0.387</b>	<b>0.495</b>	<b>0.521</b>	<b>0.631</b>

**KDD-2018.** Table 4 shows that our proposed method again achieves significant improvements over the traditional methods and the RNN-based MTSI method which reported the best number on this dataset so far.

**METR-LA.** Table 5 shows that for the forecasting task, our CDSA method outperforms previous methods in most cases. In particular, our method demonstrates clear improvement at long-term forecasting such as 60 min. This again confirms the effectiveness of directly modeling the relationship between two distant data values using self-attention mechanism.

Table 5: MAE/RMSE/MAPE on dataset **METR-LA** for comparisons with SOTA

Model	15min			30min		
	MAE	RMSE	MAPE	MAE	RMSE	MAPE
FC-LSTM Sutskever et al. [2014]	3.44	6.3	9.6%	3.77	7.23	10.9%
MTSI Luo et al. [2018]	3.75	7.31	10.52%	3.89	7.73	11.04%
BRITS Cao et al. [2018]	2.86	5.46	7.49%	3.37	6.78	9.13%
DCRNN Li et al. [2018]	2.77	5.38	7.3%	3.15	6.45	8.8%
DST-GCNN Wang et al. [2018]	2.68	5.35	7.2%	<b>3.01</b>	6.23	8.52%
GaAN Zhang et al. [2018b]	<b>2.71</b>	5.24	<b>6.99%</b>	3.12	6.36	8.56%
<b>CDSA(ours)</b>	3.01	<b>5.08</b>	7.82%	3.14	<b>5.38</b>	<b>8.30%</b>
Model	60min			Mean		
	MAE	RMSE	MAPE	MAE	RMSE	MAPE
FC-LSTM Sutskever et al. [2014]	4.37	6.89	13.2%	3.86	7.41	11.2%
MTSI Luo et al. [2018]	4.22	8.39	12.15%	4.01	7.59	10.85%
BRITS Cao et al. [2018]	3.65	7.66	10.55%	3.32	6.96	9.47%
DCRNN Li et al. [2018]	3.60	7.59	10.50%	3.28	6.80	8.87%
DST-GCNN Wang et al. [2018]	3.41	7.47	10.25%	-	-	-
GaAN Zhang et al. [2018b]	3.6	7.6	10.5%	<b>3.16</b>	6.41	8.72%
<b>CDSA(ours)</b>	<b>3.40</b>	<b>6.27</b>	<b>9.76%</b>	<b>3.16</b>	<b>5.48</b>	<b>8.50%</b>

### 4.3 Discussions

**The effects of different training losses:** For the forecasting task in **METR-LA**, we compare the performance by setting different training loss in Table 6 and we can see the performance with RMSE as loss metric achieves the best performance.

Table 6: Comparisons of different losses in **CDSA** on **METR-LA**

Time	30min	Ave	30min	Ave	30min	Ave	30min	Ave
Metric \ Loss	RMSE		MSE		MAE		(RMSE+MAE)/2	
MAE	<b>3.14</b>	<b>3.16</b>	3.43	3.41	3.28	3.33	3.21	3.25
RMSE	<b>5.38</b>	<b>5.48</b>	6.20	6.11	5.67	5.83	5.55	5.70
MAPE	<b>8.30%</b>	<b>8.50%</b>	9.32%	9.19	8.70%	9.00%	8.53%	8.80%

**Ablation study of different cross-dimensional self-attention manners:** We compare the performance for different solutions in **CDSA** mechanism on the four datasets listed above. The way of attention modeling determines the computational efficiency. As shown in Table 1, since the *Independent* calculate dimension-specific *Value* vectors in parallel, the number of variables and FLOPs are larger than those of the *Decomposed*. As the *Joint* and the *Shared* all share the variables for each units, the number of variables is small and basically equal with each other. As the *Joint* builds an huge attention map, its FLOPs is much larger than the rest. Since the *Decomposed* draws attention maps as the *Independent* but shares *Value* as the *Joint*, it reduces the computational complexity significantly. As shown in Table 7, 7, 7, 7, we evaluate these methods on **NYC-Traffic**, **KDD-2015**, **KDD-2018** and **METR-LA** datasets and the *Decomposed* always achieves the best performance.

Table 7: Comparisons of different manners to implement **CDSA** on dataset **NYC-Traffic**.

Model \ Missing Rate	20%	30%	40%	50%	60%	70%	80%	90%
CDSA(Independent)	1.327	1.327	1.331	1.355	1.362	1.379	1.393	1.425
CDSA(Joint)	Not Applicable due to memory usage limitation							
CDSA(Shared)	1.637	1.645	1.651	1.657	1.684	1.729	1.733	1.935
<b>CDSA(Decomposed)</b>	<b>1.204</b>	<b>1.208</b>	<b>1.211</b>	<b>1.214</b>	<b>1.215</b>	<b>1.217</b>	<b>1.235</b>	<b>1.377</b>

**Attention Map Visualization:** Fig. 4 shows an PM10 imputation example in location *fangshan* at  $t_2$ . Since the pattern of PM2.5 around  $t_2$  is similar to that at  $t_1$ , the attention in orange box is high. As we can see that PM2.5 and PM10 are strongly correlated, in order to impute PM10 at  $t_2$ , our model utilizes PM10 at  $t_1$  (green arrow) and PM2.5 at  $t_1$  (blue arrow), which crosses dimensions.

Table 8: Comparisons of different manners to implement CDSA on dataset **KDD-2018**.

Model \ Missing Rate	20%	30%	40%	50%	60%	70%	80%	90%
CDSA(Independent)	0.482	0.523	0.351	0.366	0.484	0.573	.608	0.721
CDSA(Joint)	0.451	0.497	0.317	0.336	0.404	0.520	0.558	0.677
CDSA(Shared)	0.783	0.799	0.672	0.692	0.784	0.793	0.791	0.832
<b>CDSA(Decomposed)</b>	<b>0.373</b>	<b>0.393</b>	<b>0.287</b>	<b>0.291</b>	<b>0.387</b>	<b>0.495</b>	<b>0.521</b>	<b>0.631</b>

Table 9: Comparisons of different manners to implement CDSA on dataset **KDD-2015**.

Model \ Dataset	PM2.5		TEMP		HUM	
	MAE	MRE	MAE	MRE	MAE	MRE
CDSA(Independent)	11.54	16.01%	0.68	4.40%	3.19	5.42%
CDSA(Joint)	11.20	15.52%	0.65	4.27%	3.05	5.37%
CDSA(Shared)	13.85	19.26%	0.75	5.18%	3.56	6.47%
<b>CDSA(Decomposed)</b>	<b>10.67</b>	<b>14.89%</b>	<b>0.61</b>	<b>4.15%</b>	<b>2.81</b>	<b>4.92%</b>

Table 10: Comparisons of different manners to implement CDSA on dataset **METR-LA**.

Model \ Dataset	60 min			Mean		
	MAE	RMSE	MAPE	MAE	RMSE	MAPE
CDSA(Independent)	3.54	7.02	10.29%	3.25	6.29	8.81%
CDSA(Joint)	3.63	7.62	10.54%	3.30	6.83	9.43%
CDSA(Shared)	3.92	7.93	11.17%	3.53	7.33	10.26%
<b>CDSA(Decomposed)</b>	<b>3.40</b>	<b>6.27</b>	<b>9.76%</b>	<b>3.16</b>	<b>5.48</b>	<b>8.50%</b>

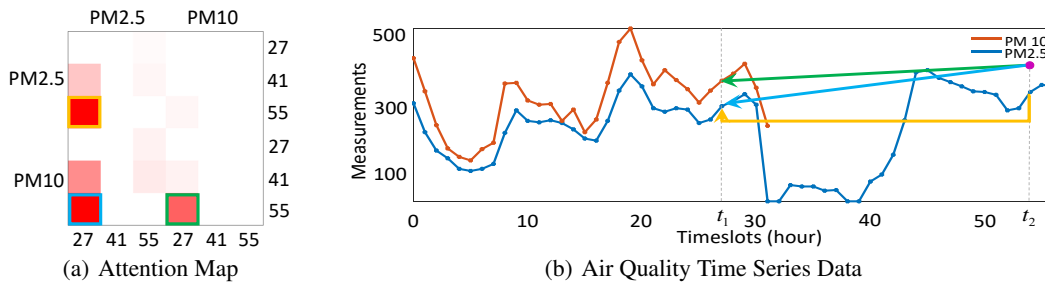


Figure 4: Visualization of the cross-dimensional self-attention on **KDD-2015**. (a) Part of *Time-Measurement* attention map. (b) Two time series of PM2.5 and PM10. The value at purple dot is missing and our model predicts its value based on other values. The arrow in (b) represents attention whose score is highlighted with bounding box in (a) of the same color.

## 5 Conclusion

In this paper, we have proposed a cross-dimensional self-attention mechanism to impute the missing values in multivariate, geo-tagged time series data. We have proposed and investigated three methods to model the crossing-dimensional self-attention. Experiments show that our proposed model achieves superior results to the state-of-the-art methods on both imputation and forecasting tasks. Given the encouraging results, we plan to extend our CDSA mechanism from multivariate, geo-tagged time series to the input that has higher dimension and involves multiple data modalities. Furthermore, we will publicly release the collected NYC-traffic dataset for future research.

## 6 Acknowledgments

This work is supported by Mitsubishi Electric.

## Bibliography

- E. Acuna and C. Rodriguez. The treatment of missing values and its effect on classifier accuracy. In *Classification, clustering, and data mining applications*, pages 639–647. Springer, 2004.
- C. F. Ansley and R. Kohn. On the estimation of arima models with missing values. In *Time series analysis of irregularly observed data*, pages 9–37. Springer, 1984.
- S. v. Buuren and K. Groothuis-Oudshoorn. mice: Multivariate imputation by chained equations in r. *Journal of statistical software*, pages 1–68, 2010.
- J.-F. Cai, E. J. Candès, and Z. Shen. A singular value thresholding algorithm for matrix completion. *SIAM Journal on Optimization*, 20(4):1956–1982, 2010.
- W. Cao, D. Wang, J. Li, H. Zhou, L. Li, and Y. Li. Brits: Bidirectional recurrent imputation for time series. In *Advances in Neural Information Processing Systems*, pages 6775–6785, 2018.
- Z. Che, S. Purushotham, K. Cho, D. Sontag, and Y. Liu. Recurrent neural networks for multivariate time series with missing values. *Scientific reports*, 8(1):6085, 2018.
- K. Cho, B. Van Merriënboer, D. Bahdanau, and Y. Bengio. On the properties of neural machine translation: Encoder-decoder approaches. *arXiv preprint arXiv:1409.1259*, 2014a.
- K. Cho, B. Van Merriënboer, C. Gulcehre, D. Bahdanau, F. Bougares, H. Schwenk, and Y. Bengio. Learning phrase representations using rnn encoder-decoder for statistical machine translation. *arXiv preprint arXiv:1406.1078*, 2014b.
- F. R. Chung and F. C. Graham. *Spectral graph theory*. American Mathematical Soc., 1997.
- K. Cup. Available on: <http://www.kdd.org/kdd2018/>, 2018.
- J. Friedman, T. Hastie, and R. Tibshirani. *The elements of statistical learning*, volume 1. Springer series in statistics New York, 2001.
- K. He, X. Zhang, S. Ren, and J. Sun. Deep residual learning for image recognition. In *Proceedings of the IEEE conference on computer vision and pattern recognition*, pages 770–778, 2016.
- S. Hochreiter and J. Schmidhuber. Long short-term memory. *Neural computation*, 9(8):1735–1780, 1997.
- H. Jagadish, J. Gehrke, A. Labrinidis, Y. Papakonstantinou, J. M. Patel, R. Ramakrishnan, and C. Shahabi. Big data and its technical challenges. *Communications of the ACM*, 57(7):86–94, 2014.
- S. Ji and J. Ye. An accelerated gradient method for trace norm minimization. In *Proceedings of the 26th annual international conference on machine learning*, pages 457–464. ACM, 2009.
- D. P. Kingma and J. Ba. Adam: A method for stochastic optimization. *arXiv preprint arXiv:1412.6980*, 2014.
- J. Lei Ba, J. R. Kiros, and G. E. Hinton. Layer normalization. *arXiv preprint arXiv:1607.06450*, 2016.
- Y. Li, R. Yu, C. Shahabi, and Y. Liu. Diffusion convolutional recurrent neural network: Data-driven traffic forecasting. In *International Conference on Learning Representations (ICLR '18)*, 2018.
- Y. Luo, X. Cai, Y. Zhang, J. Xu, et al. Multivariate time series imputation with generative adversarial networks. In *Advances in Neural Information Processing Systems*, pages 1596–1607, 2018.
- S. Ma, D. Goldfarb, and L. Chen. Fixed point and bregman iterative methods for matrix rank minimization. *Mathematical Programming*, 128(1-2):321–353, 2011.
- F. V. Nelwamondo, S. Mohamed, and T. Marwala. Missing data: A comparison of neural network and expectation maximization techniques. *Current Science*, pages 1514–1521, 2007.
- S. Ren, K. He, R. Girshick, and J. Sun. Faster r-cnn: Towards real-time object detection with region proposal networks. In *Advances in neural information processing systems*, 2015.
- L. L. Scharf and C. Demeure. *Statistical signal processing: detection, estimation, and time series analysis*, volume 63. Addison-Wesley Reading, MA, 1991.
- L. Shi. Kalman filtering over graphs: Theory and applications. *IEEE transactions on automatic control*, 54(9): 2230–2234, 2009.

- D. I. Shuman, S. K. Narang, P. Frossard, A. Ortega, and P. Vandergheynst. The emerging field of signal processing on graphs: Extending high-dimensional data analysis to networks and other irregular domains. *arXiv preprint arXiv:1211.0053*, 2012.
- R. H. Shumway and D. S. Stoffer. An approach to time series smoothing and forecasting using the em algorithm. *Journal of time series analysis*, 3(4):253–264, 1982.
- I. Silva, G. Moody, D. J. Scott, L. A. Celi, and R. G. Mark. Predicting in-hospital mortality of icu patients: The physionet/computing in cardiology challenge 2012. In *2012 Computing in Cardiology*, pages 245–248. IEEE, 2012.
- M. L. Stein. *Interpolation of spatial data: some theory for kriging*. Springer Science & Business Media, 2012.
- I. Sutskever, O. Vinyals, and Q. V. Le. Sequence to sequence learning with neural networks. In *Advances in neural information processing systems*, pages 3104–3112, 2014.
- A. Vaswani, N. Shazeer, N. Parmar, J. Uszkoreit, L. Jones, A. N. Gomez, Ł. Kaiser, and I. Polosukhin. Attention is all you need. In *Advances in neural information processing systems*, pages 5998–6008, 2017.
- P. Veličković, G. Cucurull, A. Casanova, A. Romero, P. Lio, and Y. Bengio. Graph attention networks. *arXiv preprint arXiv:1710.10903*, 2017.
- M. Wang, B. Lai, Z. Jin, X. Gong, J. Huang, and X. Hua. Dynamic spatio-temporal graph-based cnns for traffic prediction. *arXiv preprint arXiv:1812.02019*, 2018.
- Z. Yang, X. He, J. Gao, L. Deng, and A. Smola. Stacked attention networks for image question answering. In *Proceedings of the IEEE conference on computer vision and pattern recognition*, pages 21–29, 2016.
- X. Yi, Y. Zheng, J. Zhang, and T. Li. St-mvl: filling missing values in geo-sensory time series data. In *Proceedings of the 25th International Joint Conference on Artificial Intelligence*, June 2016.
- H.-F. Yu, N. Rao, and I. S. Dhillon. Temporal regularized matrix factorization for high-dimensional time series prediction. In *Advances in neural information processing systems*, pages 847–855, 2016.
- G. P. Zhang. Time series forecasting using a hybrid arima and neural network model. *Neurocomputing*, 50: 159–175, 2003.
- H. Zhang, I. Goodfellow, D. Metaxas, and A. Odena. Self-attention generative adversarial networks. *arXiv preprint arXiv:1805.08318*, 2018a.
- J. Zhang, X. Shi, J. Xie, H. Ma, I. King, and D.-Y. Yeung. Gaan: Gated attention networks for learning on large and spatiotemporal graphs. *arXiv preprint arXiv:1803.07294*, 2018b.
- Y. Zheng, X. Yi, M. Li, R. Li, Z. Shan, E. Chang, and T. Li. Forecasting fine-grained air quality based on big data. In *Proceedings of the 21th ACM SIGKDD International Conference on Knowledge Discovery and Data Mining*, pages 2267–2276. ACM, 2015.
- J. Zhou and Z. Huang. Recover missing sensor data with iterative imputing network. In *Workshops at the Thirty-Second AAAI Conference on Artificial Intelligence*, 2018.